Fabrication of Silk Fibroin/P(LLA-CL) Aligned Nanofibrous Scaffolds for Nerve Tissue Engineering

Kuihua Zhang,* Wu Jinglei, Chen Huang, Xiumei Mo*

Aligned nanofibers are an attractive option in neural tissue engineering due to providing topographic cues for cell and axonal growth. Aligned and radom 25:75 wt% silk fibroin/poly [(L-lactic acid)-*co*-(ε-caprolactone)] nanofibrous scaffolds are fabricated via electrospinning. The mechanical properties of aligned scaffolds present a strong anisotropy, with much higher tensile strength in parallel than in perpendicular direction. Schwann cell viability studies show that aligned scaffolds significantly promote cell growth and the direction of SC elongation is parallel to the direction of fibers for aligned scaffolds. These results suggest that aligned nanofibrous scaffolds might be potential candidates for nerve tissue engineering.

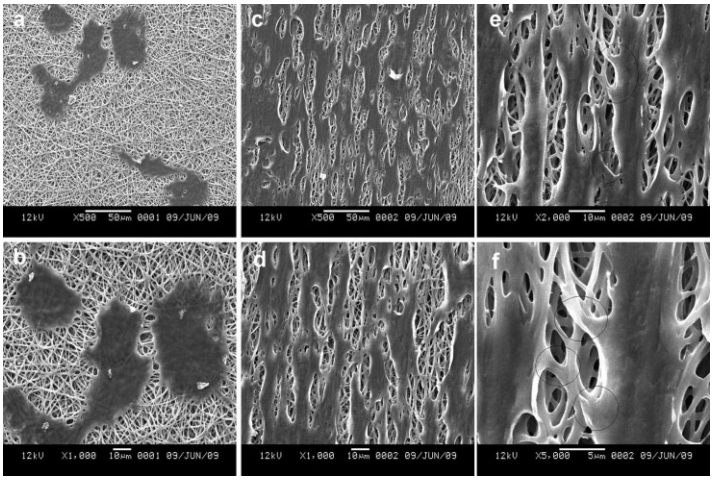

1. Introduction

Peripheral nerve regeneration and functional recovery after injury remain challenging over long-lesion gaps despite surgical interventions and entubulation of the injured nerve. Autologous nerve graft is currently the most successful method of peripheral nerve repair. However, the use of autografts for long-lesion gaps leads to many drawbacks, such as the requirement of a second surgery and the lack of available donor nerves.[1–3] Recently, electrospun nanofibrous scaffolds became a hot topic for their capacity to provide suitable environment for cell attachment, proliferation and migration, mainly because of their resemblances to the topographic features of natural extracellular matrix (ECMs).[4–6] The orientation of electrospun nanofibers plays an important role in affecting cell growth and related functions in cells such as nerve, smooth muscle and fibroblast cells.[5,7–10] The topographical cues presented by aligned electrospun nanofibers could provide better contact guidance towards neurite outgrowth.[9,11,12]

Silk fibroin (SF) as natural protein has been widely used in tissue engineering for its several unique properties including good biocompatibility, good oxygen and water vapor permeability, and biodegradability, lower inflammatory response than collagen, and commercial availability at relatively low cost.[13–15] Yang et al. reported silk fibroin has

K. Zhang
College of Materials and Textile Engineering, Jiaxing University, Zhejiang 314001, China
E-mail: zhangkuihua@126.com
W. Jinglei, C. Huang, X. Mo
Biomaterials and Tissue Engineering Laboratory, College of Chemistry and Chemical Engineering and Biological Engineering, Donghua University, Shanghai 201620, China
E-mail: med@dhu.edu.cn

DOI: 10.1002/mame.201200038

good biocompatibility with rat dorsal root ganglia (DRG) and Schwann cells (SCs) of peripheral nerve tissue.[16] However, regenerated SF possesses weak mechanical properties. In nerve tissue engineering, the scaffolds should physically resemble the nanofibrous features of ECMs with suitable mechanical properties for maintaining the stability of the scaffolds before the cells can produce their own ECMs.

Synthetic polymers, such as PLLA, PLGA and PCL, have been fabricated as random or aligned nanofibrous scaffolds, they were widely used for nerve tissue engineering due to their good biodegradability, biocompatibility and mechanical properties[17–19] Poly[(L-lactic acid)-*co*-(ε-caprolactone)] [P(LLA-CL)] is a copolymer of L-lactic acid and ε-caprolactone. Due to the controllable degradation rate and mechanical properties with different L-lactic acid/ε-caprolactone molar ratios, the potential application of electrospun P(LLA-CL) scaffolds in tissue engineering has been investigated[5,20–22] For synthetic materials, the biggest disadvantage, however, is their low hydrophilicity and lack of natural cell recognition sites[23] Recently, natural and synthetic blended nanofibrous scaffolds, including chitosan/poly(ε-caprolactone) (PCL), gelatin/PCL and collagen/PCL blends, have been studied for nerve tissue engineering[24–26] However, chitosan, gelatin and collagen are easily dissolved or swelled in water. The scaffolds of nerve guides are required to be slowly degraded with low degree of swelling, as well as suitable mechanical properties for the bearing of stresses during the surgical procedure and implantation time[27] So, the blended nanofibrous scaffolds were cross-linked by glutaraldehyde to increase their stability and strength[26]Tsai et al.[28] reported that the glutaraldehyde had remained cytoxicity to a certain extent. The conformation of SF could transform from a water soluble random coil or silk I structure into a water insoluble β-sheet or silk α structure after being treated with methanol, ethanol and water vapor[29] Therefore, aligned silk fibroin/P(LLA-CL) nanofibers may represent a potential nerve tissue engineering scaffolds with topographical structure, better biocompatibility and improved mechanical, physical and chemical properties.

Schwann cells are the primary structural and functional cells that play an important role in peripheral nerve regeneration. Once a peripheral nerve is damaged, SCs alter their morphology, behavior, and proliferation, being involved in Wallerian degeneration and Bungner bands. SCs form myelin sheaths surrounding axons to establish a channel for axonal growth.[30–32] The objective of our present study is to fabricate aligned nanofibrous scaffolds of SF and P(LLA-CL) blends and investigate their morphology and properties. SCs were further cultured on SF/P(LLA-CL) aligned nanofibrous scaffolds to evaluate the cytocompatibility.

2. Experimental Section

2.1. Materials

Cocoons of Bombyx mori silkworm were kindly supplied by Jiaxing Silk Co. Ltd (China). A copolymer of P(LLA-CL) (50:50), which has a composition of 50 mol% L-lactide, was provided by Nara Medical University(Japan). 1,1,1,3,3,3,-hexafluoro-2-propanol (HFIP) was purchased from Daikin Industries Ltd (Japan). SC lineage (RSC96) was purchased from ATCC (American). Except specially explained, all culture media and reagents were purchased from Gibco Life Technologies CO, USA.

2.2. Preparation of Regenerated SF

Raw silk was degummed three times with 0.5 wt% Na_2CO_3 solution at 100 °C for 30 min each time and then washed with distilled water. Degummed silk was dissolved in a ternary solvent system of $CaCl_2/H_2O$/EtOH solution (molar ratio 1/8/2) for 1 h at 70 °C. The solution was dialyzed with cellulose tubular membrane (250-7u; Sigma) in distilled water for 3 d at room temperature. The water was exchanged every 4 h. The SF solution was filtered and lyophilized to obtain the regenerated SF sponges.

2.3. Electrospinning

The polymer solution with the concentration of 8 wt% was prepared by dissolving SF/P(LLA-CL) blends with the weight ratio of 25:75 and pure P(LLA-CL) in HFIP solvents and stirred at room temperature for 6 h, respectively. The solution was fed into a 2.5 mL plastic syringe with a blunt-ended needle, which inner diameter was 0.4 mm. The syringe was located in a syringe pump (789100C, Cole-Pamer, America) and dispensed at a rate of 1.2 $mL \cdot h^{-1}$. A voltage of 12 kV (BGG6-358, BMEICO.LTD. China) was applied across the needle and ground collector, which was placed at a distance of 12 cm. Random nanofibers were collected on a flat collector plate wrapped with aluminum foil. Aligned nanofibers were formed using a rotating drum setup with same parameters and this rotating drum was operated at various rates to achieve different fibrous orientations (seen from Figure 1).

2.4. Characterization of Electrospun SF/P(LLA-CL) Nanofibers

The morphology was observed with a scanning electronic microscope (SEM) (JSM-5600, Japan) at an accelerated voltage of 15 kV. The mean fiber diameters and fiber orientations were estimated using an image analysis software (Image-J, National Institutes of Health, USA) and calculated by selecting 100 fibers randomly observed on the SEM images. In the angles of the nanofibers, histograms were plotted over the entire +90° to −90° range.

2.5. Pore Size Measurements

A CFP-1100-AI capillary flow porometer (PMI Porous Materials Int.) was used in this study to measure the pore size and pore size

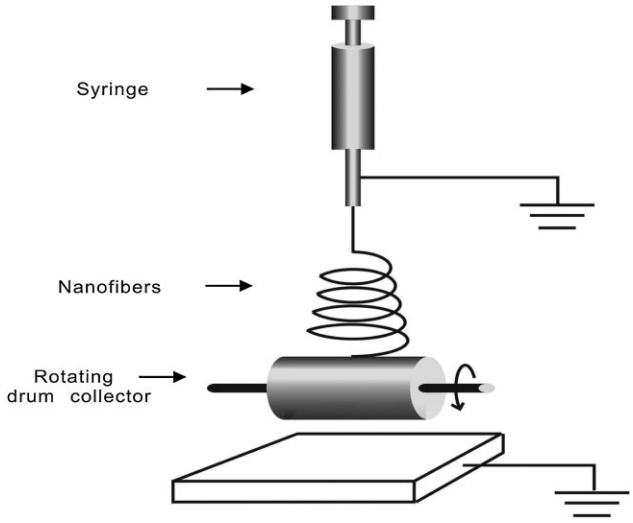

Figure 1. The experimental setup for fabricating aligned nanofibers.

distribution. Calwick with a defined surface tension of 21 dyn · cm^{-1} (PMI Porous Materials Int.) was used as the wetting agent for porometry measurements. Electrospun fibrous scaffolds were cut into 3 × 3 cm^2 squares and then soaked into the wetting agent. The soaked scaffolds were placed in adapting pan and sealed with O-rings for porometry measurement.

2.6. Mechanical Measurements

Mechanical properties were obtained by applying tensile test loads to specimens prepared from the electrospun SF/P(LLA-CL) aligned scaffolds with different fiber orientations in the parallel and perpendicular directions In this study, the specimens were prepared according to the method described by Huang et al.[33] First, a white paper was cut into template with width × gauge length, and double-side tapes were glued onto the top and bottom areas of one side. The template was then glued onto top side of the fiber scaffolds, and was cut into rectangular pieces along the vertical lines. After the aluminum foil was carefully peeled off, single side tapes were applied onto the gripping areas as end-tabs. The resulting specimens had a planar dimension of width × gauge length = 10 × 30 mm^2. Mechanical properties were tested by a materials testing machine (H5K-S, Hounsfield, England) at the temperature of 20 °C and a relative humidity of 65% and an elongation speed of 10 mm · min^{-1}. Each group was measured with three samples. The specimen thicknesses were measured using a digital micrometer, having a precision of 1 μm.

2.7. Treatment of SF/P(LLA-CL) Nanofibrous Scaffolds

The SF/P(LLA-CL) nanofibrous scaffolds were treated with 75 vol% ethanol vapor to induce a β-sheet conformational transition, which results in insolubility in water. Briefly, 75 vol% ethanol vapor treated samples were prepared by placing SF/P(LLA-CL) nanofibrous scaffolds in a desiccator saturated with 75 vol% ethanol vapor at room temperature for 6 h and then dried in vacuum at room temperature for 24 h.

2.8. Viability Study of SCs on Electrospun Scaffolds

2.8.1. Cell Proliferation

Electrospun scaffolds were prepared on circular glass coverslips (14 mm in diameter) and fixed the coverslips into 24-well plates with stainless ring. Before seeding cells, scaffolds were sterilized by immersion in 75% ethanol for 2 h, washed three times with phosphate-buffered saline (PBS), and then washed once with the culture medium. SCs were seeded at a density of 1.0 × 10^4 cells per well onto fiber scaffolds and control glass coverslips ($n = 3$). The SCs proliferated for 1, 3, 5, and 7 d, at which time the number of attached cells was again determined by 3-[4,5-dimehyl-2-thiazolyl]-2, 5-diphenyl-2H-tetrazolium bromide (MTT).

Cells viability on different substrates was determined by MTT method. Briefly, the cells were incubated with 5 mg · mL^{-1} MTT for 4 h. Thereafter, the culture media were extracted and 400 μL dimethyl sulfoxide (DMSO) was added in each sample for about 20 min. When the crystal was sufficiently dissolved, aliquots were pipetted into the wells of a 96-well plate and tested by an Enzyme-labeled Instrument (MK3, Thermo, USA), and the absorbance at 490 nm for each well was measured.

2.8.2. Cell Morphology

After 3 d of culturing, the electrospun fibrous scaffolds with cells were examined by SEM. The scaffolds were rinsed twice with PBS and fixed in 4% glutaraldehyde water solution at 4 °C for 2 h. Fixed samples were rinsed twice with PBS and then dehydrated through a series of graded ethanol solutions (30, 50, 70, 80, 90, 95, and 100%). Finally, they were dried in vacuum overnight. The dry cellular constructs were sputter coated with gold and observed under SEM at a voltage of 10 kV.

2.9. Statistical Analysis

Statistical analysis was performed using Origin 7.5 (Origin Lab Inc., USA). Statistical comparisons were determined by the analysis of One-Way ANOVA. In all evaluations, $p < 0.05$ was considered as statistically significant.

3. Results and Discussion

3.1. Morphology of the Electrospun SF/P(LLA-CL) Nanofibrous Scaffolds

The alignment of nanofibers plays a dominant role in improving the adhesion, proliferation and migration of nerve cells as well as neurite growth.[34] Highly aligned nanofibers were also conducive to neurite growth in comparison with intermediate or random oriented counterparts.[17] The 8% (w/v) SF/P(LLA-CL) blended solution was

electrospun onto a rotating drum at different rotation rates from 500 to 4000 rpm to form various fiber orientations. SEM images and fiber angles distribution of electrospun nanofibers were shown in Figure 2. The orientation was observed as the rotation rates increased. At the rotating rate of 500 rpm, the nanofibers were random. The nanofibers of the angles between −20 and +20° accounted for 38, 60, 88, and 90% when the rotating rate was 1000, 2000, 3000, and 4000 rpm, respectively. The alignment of nanofibers obviously increased with the increase of the rotating rates. The mean diameters of electrospun SF/P(LLA-CL) nanofibers at different rotating rates were shown in Table 1. The rotation speed of the rotating drum did not markedly influence the nanofiber diameter. To compare with electrospun SF/P(LLA-CL) aligned nanofibers, the electrospun P(LLA-CL) aligned fibers at rotating rate of 4000 rpm were fabricated and the data were shown in Figure 3 and Table 1. The fibers of the angles between −20 and +20°

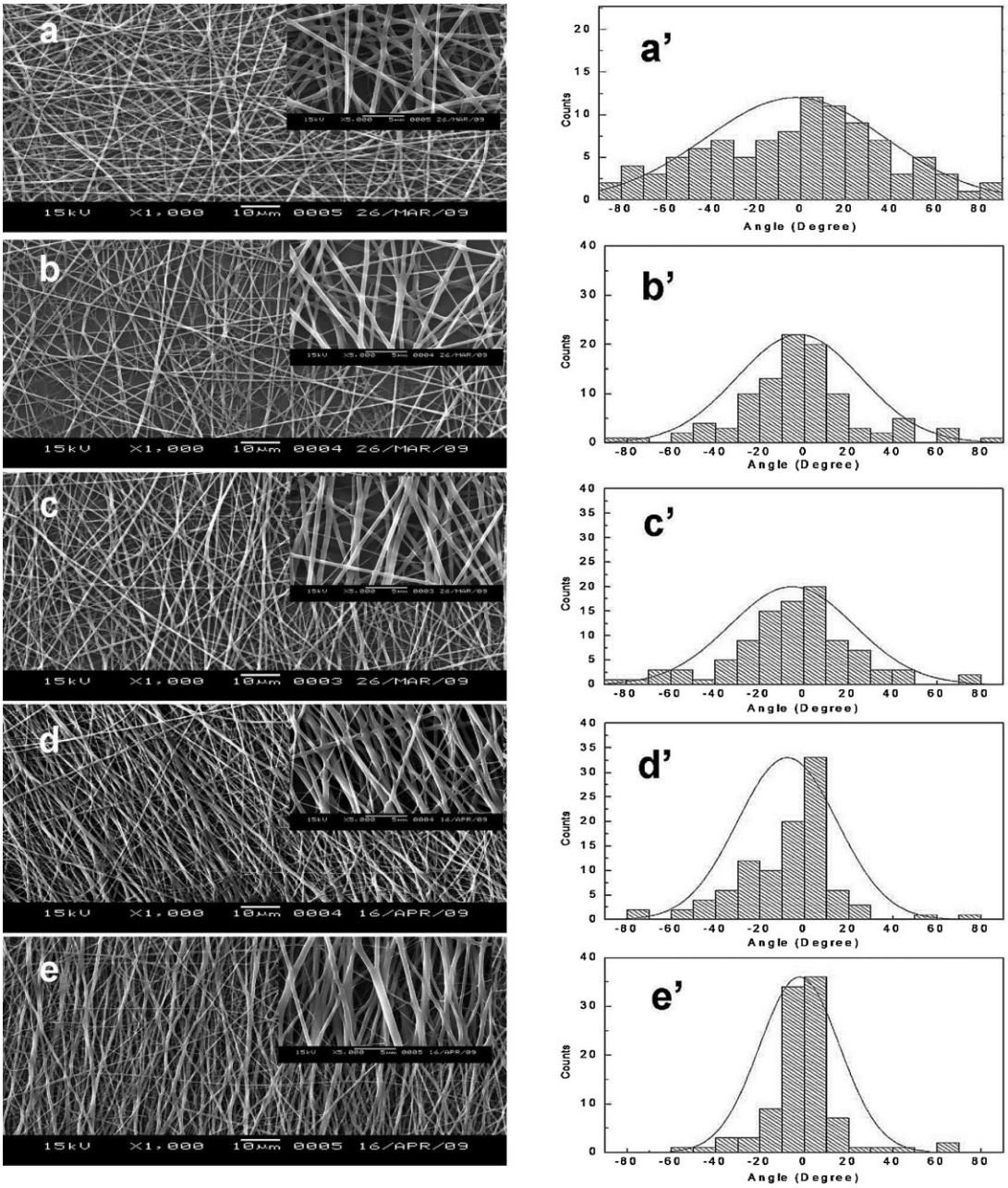

Figure 2. SEM images and the angle distribution of electrospun SF/P(LLA-CL) nanofibers for different rates of rotation. (a, a') 500; (b, b') 1000; (c, c') 2000; (d, d') 3000; (e, e') 4000 rpm.

Table 1. Average fiber diameter of electrospun SF/P(LLA-CL) and P(LLA-CL) with different rotation rates.

Rotation rate [rpm]	Fiber diameter [nm]
500	392 ± 105
1000	385 ± 121
2000	394 ± 102
3000	381 ± 124
4000	391 ± 112
4000 (PLLA-CL)	1095 ± 368

accounted for 94% and the mean diameter of aligned fibers was much larger than that of the SF/P(LLA-CL) aligned fibers obtained from the same processing conditions. The result was in consistent with the comparison of electrospun random SF/P(LLA-CL) and P(LLA-CL) fibers.[33]

3.2. Pore Diameter Analyses

Microscale and nanoscale porous structure of electrospun nanofibrous scaffolds play pivotal roles for cellular growth and tissue regeneration.[35] Pore diameter distribution, pore diameters of random and aligned (4000 rpm) SF/P(LLA-CL) and P(LLA-CL) electrospun fibrous scaffolds were shown and summarized in Figure 4 and Table 2. The results showed that the pore diameter distribution, pore diameters of random and aligned SF/P(LLA-CL) exist minute differences and the reason might be that the orientation degree of aligned fibers collected by rotating drum was not highly uniform. SEM observed that the fibers had a solid surface with interconnected voids, so that a porous structure was present. However, the pore diameter distribution and pore diameters of random and aligned P(LLA-CL) electrospun fibrous scaffolds had obvious difference, random is much larger than that of aligned. This may be caused the fact that the mean diameter of aligned P(LLA-CL) electrospun fibers(1095 nm) was much thicker than that of aligned SF/P(LLA-CL) electrospun fibers(409 nm).[33,36] We observed a large amount of fibers accumulated disorderly and bonded together in random P(LLA-CL) electrospun fibrous scaffolds (seen from Figure 5). Therefore, the pore structure of scaffolds might be jammed with increasing the thickness of scaffolds. Furthermore, the thickness of random P(LLA-CL) was more than that of aligned one from Table 2.

3.3. Mechanical Properties Analyses

The typical tensile stress/strain curves of SF/P(LLA-CL) aligned nanofibrous scaffolds were shown in Figure 6. The average elongation at break and average tensile strength of each specimen were summarized in Table 3. Figure 6 and Table 3 showed that the typical tensile stress/strain curves of SF/P(LLA-CL) aligned nanofibrous scaffolds had significant difference between parallel and perpendicular directions. The elongation at break and the tensile strength were 345.35 ± 15.84% and 7.56 ± 0.389 MPa, respectively. At parallel direction, the elongation at break and the tensile strength were 320.56 ± 41.68% and 25.78 ± 5.25 MPa, respectively. The results clarified that the SF/P(LLA-CL) aligned nanofibrous scaffolds had much higher tensile

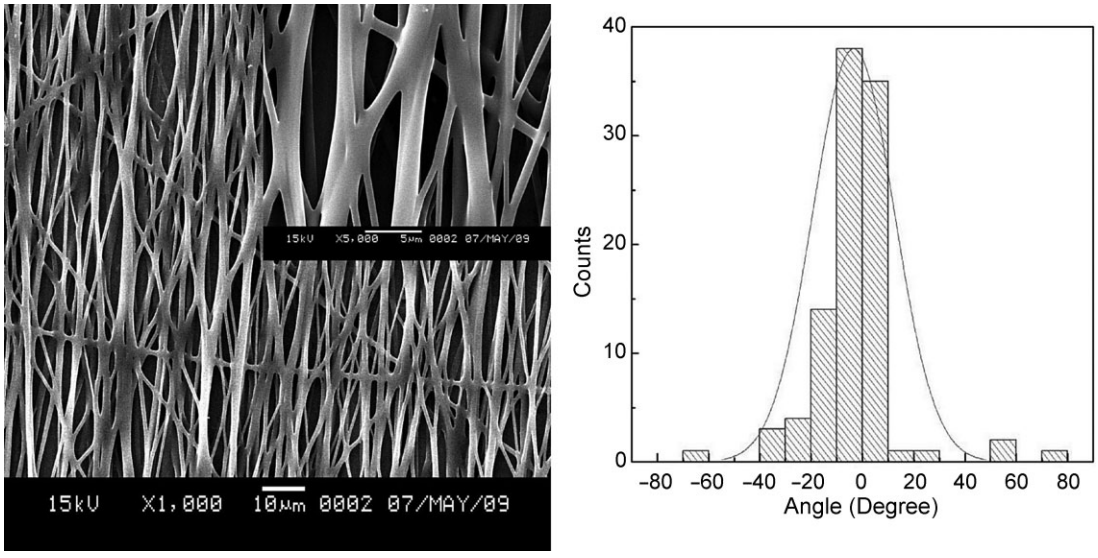

Figure 3. SEM images and the angle distribution of electrospun P(LLA-CL) fibers for 4000 rpm.

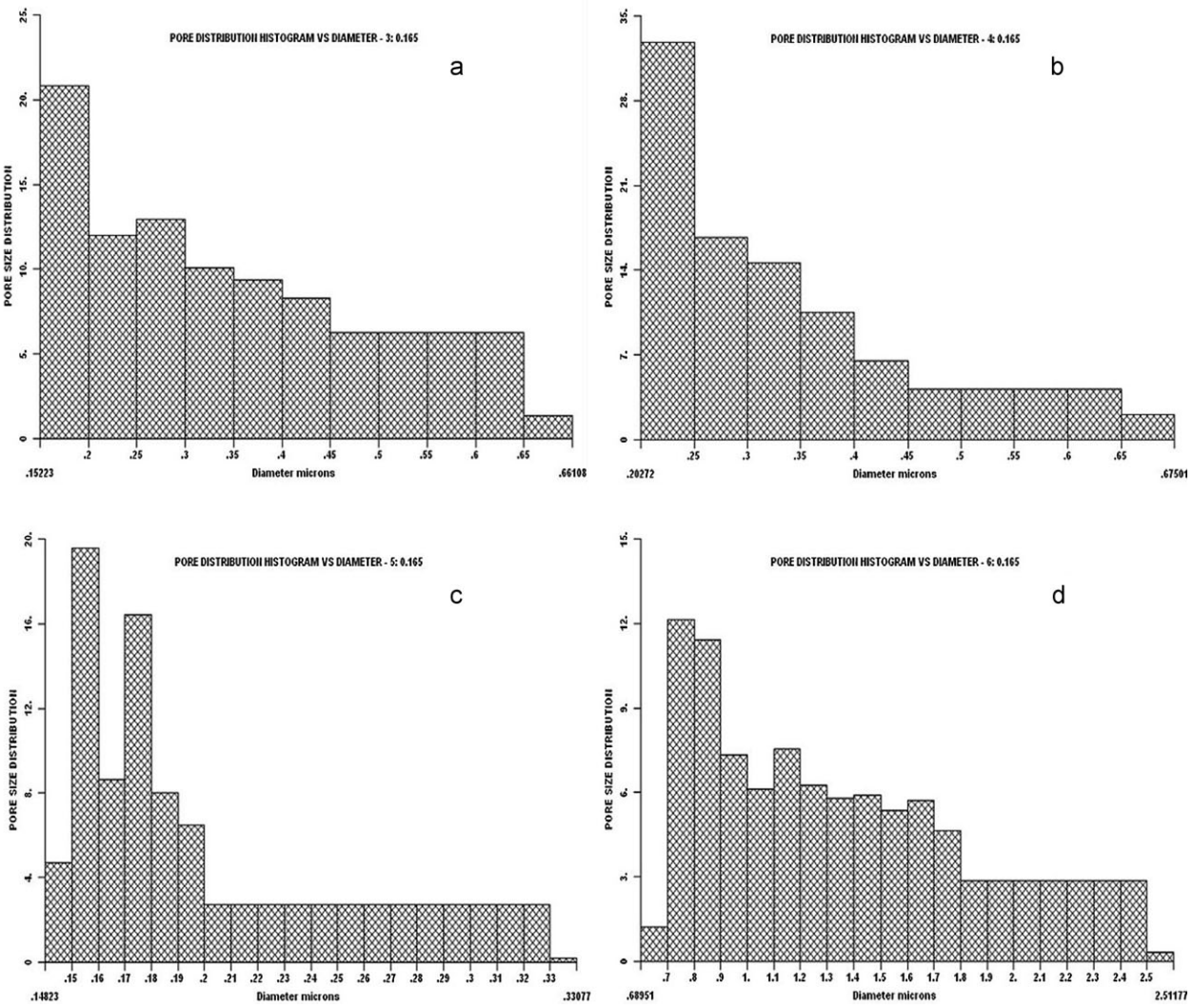

Figure 4. The pore diameter distribution of electrospun SF/P(LLA-CL) and P(LLA-CL) fibrous scaffolds. (a) SF/P(LLA-CL) random; (b) SF/P(LLA-CL) aligned; (c) P(LLA-CL) random; (d) P(LLA-CL) aligned.

strength at parallel direction than at perpendicular direction. However, the elongation at break did not show distinct difference both at parallel and perpendicular directions. This is possibly because many of the small branches fibers combine the parallel fibers together (seen from Figure 2e), which helped the scaffolds to withstand higher stress. Meanwhile, P(LLA-CL) possessed good viscoelasticity to resist higher stress without laceration.

Table 2. Pore diameter of SF/P(LLA-CL) and P(LLA-CL) fibrous scaffolds.

Sample	Morphology	Specimen thickness [mm]	Mean flow pore diameter ± SD [μm]	Largest pore diameter [μm]	Smallest pore diameter [μm]
SF/P(LLA-CL)	random	0.067	0.3193 ± 0.127	0.6611	0.1540
	aligned	0.059	0.3013 ± 0.0986	0.6750	0.2027
P(LLA-CL)	random	0.130	0.1803 ± 0.0322	0.3308	0.1482
	aligned	0.070	1.2642 ± 0.4413	2.5118	0.4413

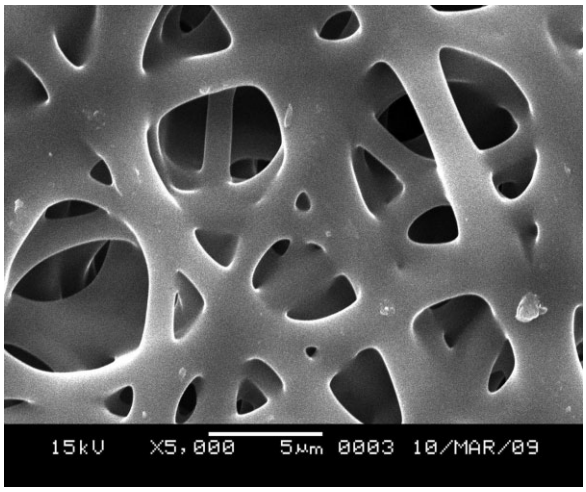

Figure 5. SEM images of random electrospun P(LLA-CL) fibers.

3.4. Viability of SCs on Electrospun Scaffolds

Cultured on SCs electrospun scaffolds might serve as a model for denervated SCs in the distal stump of an injured nerve.[37] Proliferation of SCs cultured on different electrospun scaffolds was determined by MTT assay after culturing for 1 3, 5, and 7 d and was shown in Figure 7. All electrospun scaffolds had good cell viability in comparison with coverslips. Cell proliferation on SF/P(LLA-CL) aligned or random nanofibrous scaffolds exhibited significant difference ($p < 0.05$) comparing to P(LLA-CL) aligned or random fibrous scaffolds. Meanwhile, cell proliferation on SF/P(LLA-CL) aligned nanofibrous scaffolds was superior to random nanofibrous scaffolds ($p < 0.05$). Possible reason was that the mechanical stretching of the aligned nanofibers gave rise to better SCs proliferation. In addition, cells occupied more compactly the space due to the guidance of regular alignment on SF/P(LLA-CL) aligned nanofibrous scaffolds.[38] Tissue-culture polystyrene (TCP) is normally treated by sufficient amounts of trace ECM proteins from serum-supplemented media to promote cell attachment.[39] Therefore, cells had greater proliferation on TCP than on electrospun P(LLA-CL) fibrous scaffolds.

Cell morphology and the interaction between cells and electrospun scaffolds were studied in vitro for 3 d. SEM micrographs were shown in Figure 8 and 9. After 3 d, the SCs were found to integrate well with the surrounding fibers and elongated parallel along the fiber orientation on SF/P(LLA-CL) aligned nanofibrous scaffolds. Some pseudopodia stretched from the edge of the elongated cell body. They helped cells to attach to the surrounding fibers and produced a "bridge" between cell body and nanofibers (Figure 8e and f). These pseudopodia fused cells with fibers

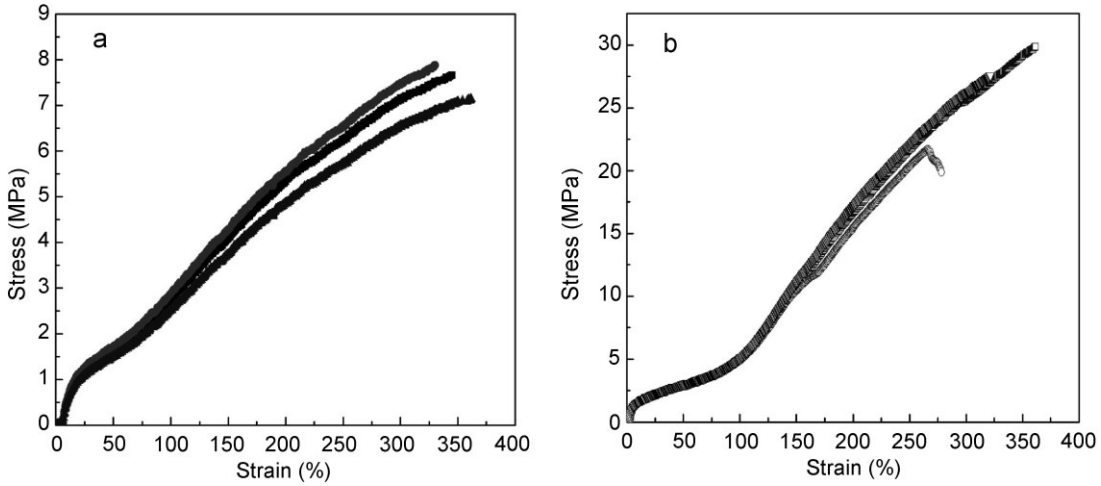

Figure 6. Stress/strain curves of electrospun SF/P(LLA-CL) aligned scaffolds. (a) Aligned (perpendicular); (b) aligned (parallel).

Table 3. Mechanical properties of electrospun SF/P(LLA-CL) aligned nanofibrous scaffolds.

SF/P(LLA-CL) aligned nanofibrous scaffolds	Specimen thickness [mm]	Elongation at break [%]	Tensile strength [MPa]
aligned (parallel)	0.109 ± 0.003	320.56 ± 41.68	25.78 ± 5.25
aligned (perpendicular)	0.112 ± 0.008	345.35 ± 15.84	7.56 ± 0.38

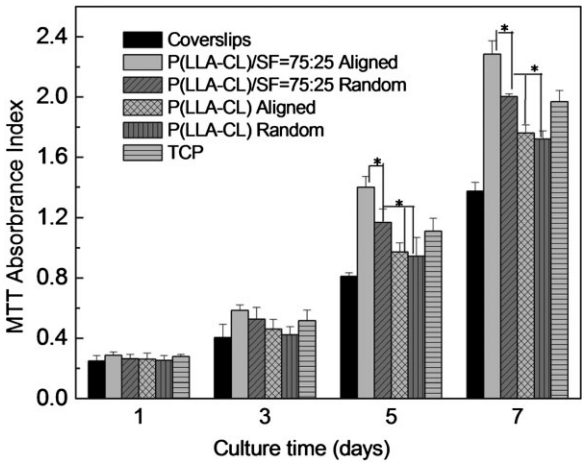

Figure 7. Proliferation of SCs cultured on electrospun scaffolds for 1, 3, 5, and 7 d. Data are expressed as mean ± SD ($n = 3$). Statistical difference between groups is indicated (*, $p < 0.05$).

to contribute to both communicating intracellular signals and promoting cells adhesion and migration on aligned direction. In contrast, the SCs spread at all directions on SF/P(LLA-CL) random nanofibrous scaffolds. Meanwhile, we found surprisingly that the fiber alignment had no significant effect on the SCs and cells did not elongate parallel along the fiber orientation but spread at all directions on P(LLA-CL) aligned fibers scaffolds. This may be caused by the large fibrous diameter (1095 nm) of electrospun P(LLA-CL), which could not provide good contact guidance. Corey et al.[17] demonstrated cells grew faster on the aligned nanofibers than on aligned microfibers.

Surface chemistry and topography of the tissue engineering scaffolds play major roles in regulating cell behavior, including cell adhesion, cell proliferation, cell differentiation, cell orientation, cell motility, surface antigen display, cytoskeletal condensation, activation of tyrosine kinases, and modulation of intracellular signaling pathways that regulate transcriptional activity and gene expression.[40] Previous studies have proved that terminal chemical functional groups can control cell growth or differentiation and modulate the structure and molecular composition of cell/matrix adhesions as well as focal adhesion kinase (FAK) signaling.[41,42] Electrospun nanofibrous scaffolds provides a powerful mechanism to encourage and direct cell behavior ranging from cell adhesion to gene expression and controlled alignment of fibers can direct cell orientation and migration.[40] The SF/P(LLA-CL) aligned nanofibrous scaffolds incorporated functional groups such as NH_2, COOH, and OH onto their surfaces through adding SF, which could introduce cell recognition

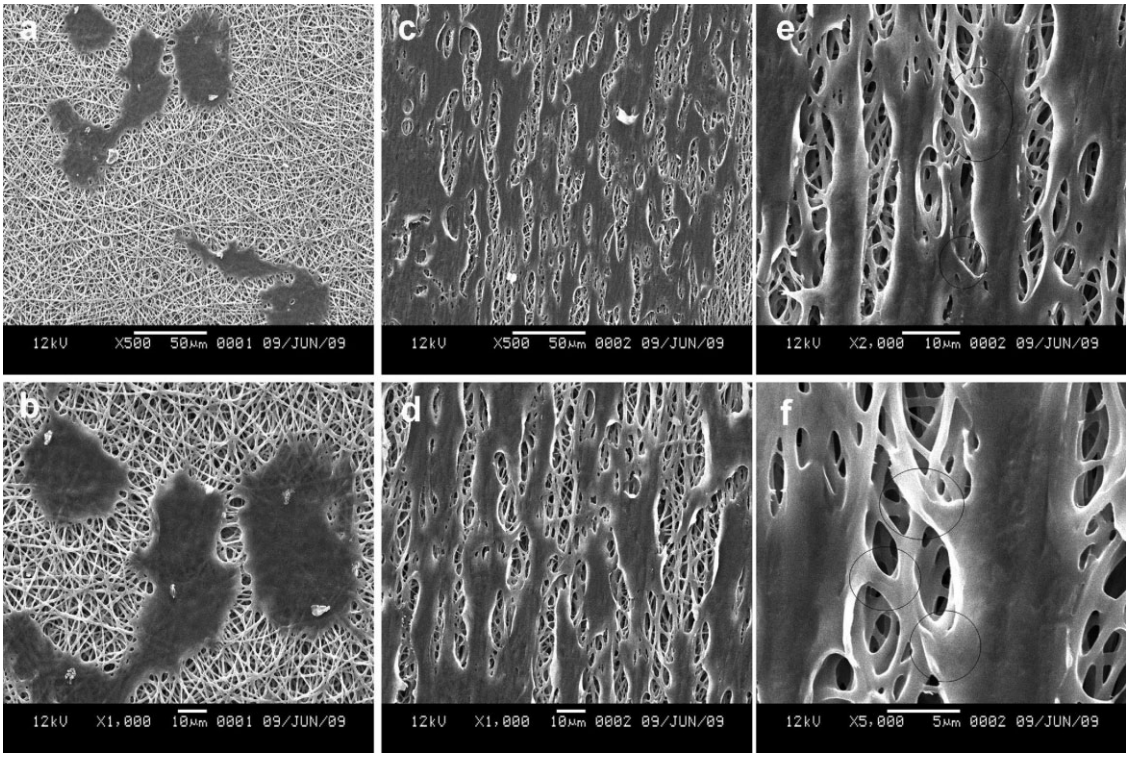

Figure 8. Morphology of SCs on random SF/P(LLA-CL) scaffolds [magnification: (a) 500; (b) 1000×]; aligned SF/P(LLA-CL) scaffolds [magnification: (c) 500; (d) 1000; (e) 2000; (f) 5000×].

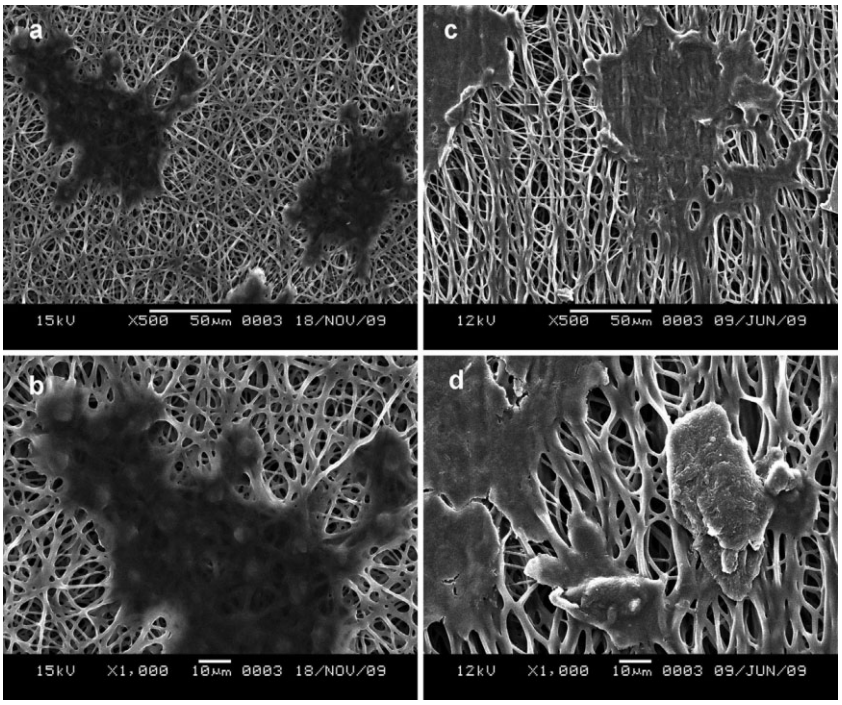

Figure 9. Morphology of SCs on random P(LLA-CL) scaffolds [magnification: (a) 500; (b) 1000×]; aligned P(LLA-CL) scaffolds [magnification: (c) 500; (d) 1000×].

sites to promote cell/material interactions. Meanwhile, nanoscale and alignment of fibers provided topographic cues for cell growth.

4. Conclusion

In the present study, we produced a biocomposite SF/P(LLA-CL) aligned nanofibrous scaffolds with a ratio of 25:75 wt% by electrospinning technique under optimum condition. The mean flow diameter of aligned SF/P(LLA-CL) nanofibrous scaffolds was similar to that of random. The mechanical properties of SF/P(LLA-CL) aligned nanofibrous scaffolds existed in anisotropy, the SF/P(LLA-CL) aligned nanofibrous scaffolds had much higher tensile strength at parallel than perpendicular direction. The aligned SF/P(LLA-CL) nanofibrous scaffolds could provide not only chemistry cues but also topographic cues of nanoscale and alignment for SCs growth. Therefore, the results showed that SF/P(LLA-CL) aligned nanofibrous scaffolds supported greater SCs growth and regulated cell orientation. This type of scaffolds may have the potential of application in nerve tissue engineering.

Acknowledgements: This research was supported by a program of the Zhejiang Education Office (Y201122407). Science and Technology Commission of Jiaxing Municipality Program (2010AY1089), National Natural Science Foundation of China (31070871).

Received: February 9, 2012; Revised: June 25, 2012; Published online: October 22, 2012; DOI: 10.1002/mame.201200038

Keywords: aligned nanofibrous scaffolds; electrospinning; nerve tissue engineering; SF/P(LLA-CL) blends

[1] Y. F. Susan, G. Tessa, *Mol. Neurobiol.* **1997**, *14*, 67.
[2] P. C. Francel, K. S. Smith, F. A. Stevens, S. C. Kim, J. Gossett, M. E. Davis, M. Lenaerts, P. Tompkins, *J. Neurosurg.* **2003**, *99*, 549.
[3] S. G. Wang, Q. Cai, J. W. Hou, J. Z. Bei, T. Zhang, J. Yang, Y. Q. Wan, *J. Biomed. Mater. Res. Part A* **2002**, *66*, 522.
[4] D. H. Reneker, I. Chun, *Nanotechnology* **1996**, *7*, 216.
[5] C. Y. Xu, R. Inai, M. Kotaki, S. Ramakrishna, *Biomaterials* **2003**, *25*, 877.
[6] Z. Ma, M. Kotaki, R. Inai, S. Ramakrishna, *Tissue Eng.* **2005**, *11*, 101.
[7] S. Y. Chew, R. Mi, A. Hoke, K. W. Leong, *Adv. Funct. Mater.* **2007**, *17*, 288.
[8] H. B. Wang, M. E. Mullins, J. M. Cregg, A. Hurtado, M. Oudega, M. T. Trombley, R. J. Gilbert, *J. Neural. Eng.* **2009**, *6*, 1.
[9] E. Schnell, K. Klinkhammer, S. Balzer, G. Brook, D. Kleeb, P. Dalton, J. Mey, *Biomaterials* **2007**, *28*, 3012.
[10] C. H. Lee, H. J. Shin, I. H. Cho, Y. M. Kang, I. A. Kim, K. D. Park, I. A. Kim, K. D. Park, J. W. Shin, *Biomaterials* **2005**, *26*, 1261.
[11] S. Y. Chew, R. Mi, A. Hoke, K. W. Leong, *Biomaterials* **2008**, *29*, 653.
[12] J. Gerardo-Naval, T. Führmann, K. Klinkhammer, N. Seiler, J. Mey, D. Klee, M. Möller, P. D. Dalton, G. A. Brook, *Nanomedicine*, **2009**, *4*, 11.
[13] R. L. Horan, K. Antle, A. L. Collette, Y. Z. Wang, J. Huang, J. E. Moreau, V. Volloch, D. L. Kaplan, G. H. Altman, *Biomaterials* **2005**, *26*, 3385.
[14] A. R. Murphy, P. S. John, D. L. Kaplan, *Biomaterials* **2008**, *29*, 2829.
[15] L. Meinel, S. Hofmann, V. Karageorgiou, C. K. Head, J. McCool, G. Gronowicz, L. Zichner, R. Langer, G. V. Novakovic, D. L. Kaplan, *Biomaterials* **2005**, *26*, 147.
[16] Y. M. Yang, F. Ding, J. Wu, W. Hu, W. Liu, J. Liu, X. S. Gu, *Biomaterials* **2007**, *28*, 5526.
[17] J. M. Corey, D. Y. Lin, K. B. Mycek, Q. R. Chen, S. Samuel, E. L. Feldman, D. C. Martin, *J. Biomed. Mater. Res. Part A* **2007**, *83*, 636.
[18] T. B. Bini, S. J. Gao, T. C. Tan, S. Wang, A. Lim, L. B. Hai, S. Ramakrishna, *Nanotechnology* **2004**, *15*, 1459.
[19] J. W. Xie, S. M. Willerth, X. R. Li, M. R. Macewan, A. Rader, S. E. Sakiyama-Elber, Y. N. Xia, *Biomaterials* **2009**, *30*, 354.
[20] I. K. Kwon, S. Kidoaki, T. Matsuda, *Biomaterials* **2005**, *26*, 3929.

[21] X. M. Mo, Y. Xu, M. Kotaki, H. J. Weber, S. Ramakrishna, *Polym. Prepr. Am. Chem. Soc. Div. Polym. Chem.*, **2003**, *44*, 128.
[22] X. M. Mo, C. Y. Xu, M. Kotaki, S. Ramakrishna, *Biomaterials* **2004**, *25*, 1883.
[23] B. S. Kim, D. J. Mooney, *Trends Biotechnol.* **1998**, *16*, 224.
[24] M. P. Prabhakaran, J. R. Venugopal, T. T. Chyan, L. B. Hai, C. K. Chan, A. Y. Lim, S. Ramakrishna, *Tissue Eng.* **2008**, *14*, 1787.
[25] L. Ghasemi-Mobarakeh, M. P. Prabhakaran, M. Morshed, M. Nasr-Esfahanid, S. Ramakrishn, *Biomaterials* **2008**, *29*, 4532.
[26] J. S. Choi, S. J. Lee, G. J. Christ, A. Atala, J. J. Yoo, *Biomaterials* **2008**, *29*, 2899.
[27] G. Ciardelli, V. Chiono, *Macromol. Biosci.* **2006**, *6*, 13.
[28] C. C. Tsai, R. N. Huang, H. W. Sung, H. C. Liang, *J. Biomed. Mater. Res.* **2000**, *52*, 58.
[29] A. J. Meinela, K. E. Kubow, E. Klotzsch, M. Garcia-Fuentesa, M. L. Smith, V. Vogel, H. P. Merkle, L. Meinela, *Biomaterials* **2009**, *30*, 3058.
[30] C. A. Krekoski, D. Neubauer, J. Zuo, D. Muir, *Axonal J. Neurosci.* **2001**, *21*, 6206.
[31] A. Mosahebi, M. Wiberg, G. Terenghi, *Tissue Eng.* **2003**, *9*, 209.
[32] Y. Yang, X. Chen, F. Ding, P. Zhang, J. Liu, X. Gu, *Biomaterials* **2007**, *28*, 1616.
[33] K. H. Zhang, H. S. Wang, C. Huang, Y. Su, X. M. Mo, I. Yoshito, *Mater. Res. : Part A* **2010**, *93A*, 984.
[34] L. M. Y. Yu, N. D. Leipzig, M. S. Shoichet, *Mater. Today* **2008**, *11*, 536.
[35] S. J. Eichhorn, W. W. Sampson, *J. R. Soc. Interface* **2005**, *2*, 309.
[36] D. P. Li, M. W. Frey, Y. L. Joo, *J. Membr. Sci.* **2006**, *286*, 104.
[37] R. Mirsky, P. R. Jessen, *Brain Pathol.* **1999**, *9*, 293.
[38] S. P. Zhong, W. E. Teo, X. Zhu, W. Roger, S. Ramakrishna, *J. Biomed. Mater. Res. Part A* **2009**, *79*, 456.
[39] F. Yang, C. Y. Xu, M. Kotaki, S. Wang, S. Ramakrishna, *J. Biomater. Sci. Polym. Ed.* **2004**, *15*, 1483.
[40] M. M. Stevens, J. H. George, *Science*, **2005**, *310*, 1135.
[41] N. Faucheux, R. Schweiss, K. Lutzow, C. Werner, T. Groth, *Biomaterials* **2004**, *25*, 2721.
[42] B. G. Keselowsky, D. M. Collard, A. J. Garcia, *Biomaterials* **2004**, *25*, 5947.